2-D Ray-Tracing Approach for the Design of 3-D Dome Arrays Considering Mutual Coupling

María Pubill-Font*, Francisco Mesa†, Astrid Algaba-Brazález‡, Can Ding*, and Oscar Quevedo-Teruel§
*Global Big Data Technologies Centre, Univ. of Technology Sydney, Sydney, Australia, maria.pubillfont@student.uts.edu.au
†Departament of Applied Physics 1, E.T.S. de Ingeniería Informática, University of Sevilla, Seville, Spain.
‡Department of Communication and Information Technologies, Polytechnic University of Cartagena, Cartagena, Spain
§Division of Electromagnetic Engineering and Fusion Science, KTH Royal Institute of Technology, Stockholm, Sweden

***Abstract*—The integration of lenses with array antennas (referred to as dome arrays) in future communication systems offers numerous benefits, including improved radiation efficiency, adaptability in different use cases, and reduced energy consumption. This article elaborates upon using a novel two-dimensional ray-tracing technique for rapid and accurate numerical evaluation of the far-field radiation properties of three-dimensional multilayer dome arrays. Moreover, we also investigate how to account in our model for the effect of mutual coupling in dome arrays. The accuracy of the method is validated by comparing the simulated radiation patterns from the proposed ray-tracing model with results generated by widely used full-wave simulation tools like CST.**

***Index Terms*—Dome arrays, lenses, losses, mutual coupling, phased array antennas, radiation pattern, ray tracing.**

I. Introduction

The next-generation of terrestrial and satellite communication systems operating at frequencies beyond millimeter waves face significant hardware constraints that influence the selection of antenna technologies [1]. At these high frequencies, limitations arise from high free-space path loss, increased material losses, significant atmospheric absorption, and limited output power due to immature semiconductor technology [2]. Therefore, efficient antennas that can provide high gain, beam scanning, and wideband performance are crucial for future radio access systems [3]–[5]. By combining quasi-optical antennas [6], [7] and traditional phased array antennas (PAA) [8], [9], we can exploit the advantages of both antenna technologies that comprise the so-called dome arrays [10].

Dielectric lenses integrated with PAA exhibit interesting properties that may be applied in a wide range of scenarios: reconfigurability of the radiation performance of a PAA depending on the use case [10], increasing the beam scanning range [11], [12], suppression of the level of the grating lobe [13], and implementation of energy-efficient systems [14].

One of the key drawbacks when designing and optimizing dome arrays by employing commercial full-wave simulators is the large amount of computational resources required because of the substantial electrical dimensions of the dielectric lens. In fact, ray-tracing-based simulation tools are preferred for evaluating the radiating performance of lens antennas, as they save both time and computational resources [15]–[22]. In [23], an effective, accurate and simple two-dimensional (2-D) ray-tracing tool is introduced to assess the radiation patterns in the far field of multilayer dielectric dome antennas. This tool accounts for reflection and absorption losses, as well as the inclusion of matching layers to mitigate reflection losses. It demonstrates that 2-D models based on geometrical optics may provide valuable insights and a suitable initial starting point toward the development of practical three-dimensional (3-D) dome array antennas.

In this work, we adapt the 2-D ray-tracing model presented in [23] and further investigate its application in the numerical evaluation of the radiation performance of 3-D dome array antennas. Additionally, the proposed ray-tracing approach incorporates the effect of mutual coupling among the antenna elements of the PAA. Mutual coupling is a critical factor in MIMO communications and radio access systems with duplex capabilities, such as the sub-band full-duplex (SBFD) schemes proposed for future radio access base stations [24], [25]. Therefore, efficient ray-tracing modeling tools that account for mutual coupling and isolation in integrated radio front-ends are essential for accurate and fast numerical evaluation of the system radiating performance. Finally, our presented method is validated through a comparison of the far-field patterns obtained with the proposed ray-tracing model with those that resulted from CST Studio Suite.

II. Ray-Tracing Model

In this section, we outline our implementation of a simplified 2-D ray-tracing model applied to analyze the radiation performance of homogeneous dielectric lenses combined with arrays. This model uses geometric optics (GO) principles to simulate the behavior of electromagnetic waves, significantly reducing computational time compared to traditional full-wave simulations. The geometry of the dome used to validate the 2-D ray-tracing model and the key parameters involved in the far-field evaluation are illustrated in Fig. 1. The boundaries of the lens are two conic lower and upper surfaces, S_1 and S_2, whose height is defined in terms of the cylindrical radial coordinate ρ as

$$z_i(\rho) = h_i + \frac{c_i \rho^2}{1 + \sqrt{1 - (1 + K_i) c_i^2 \rho^2}} \tag{1}$$

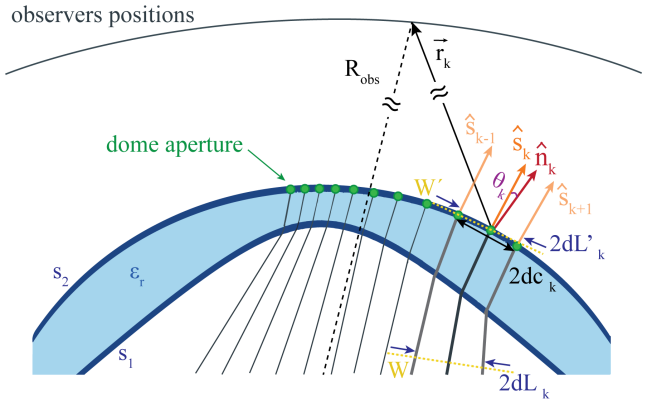

Fig. 1: Dome array configuration and main parameters involved in ray-tracing model.

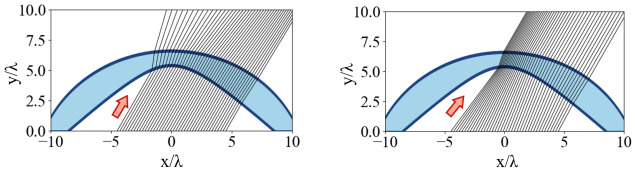

Fig. 2: Example of rays computed with *direct RT* with different phase array excitations. (a) Linear phase array excitation. (b) Phase array excitation from *reverse RT*.

where h_i is the height at $\rho = 0$, c_i is the curvature, and K_i is the conic constant. The surfaces S_1 and S_2 have been optimized using our model to achieve a flat gain across all scanning angles. The optimized parameters of the dielectric lens are: $c_1 = -0.025$, $K_1 = -2.2$, $h_1 = 5.5\lambda$, $c_2 = -0.007$, $K_2 = -0.2$, and $h_2 = 6.5\lambda$. The lens is made of a homogeneous dielectric material with $\varepsilon_r = 2.5$, and two quarter-wavelength matching layers to prevent reflections. The dome is placed on top of an array of length L = 103.8 mm, working at a central frequency of 26 GHz.

The ray-tracing model can be divided into three steps: GO, ray tube power theory, and the Kirchhoff diffraction formula [19], [23]. GO is used to obtain the rays' trajectories through the lens by making use of the Snell-Descartes law at each change of medium [26]. This procedure is used in two different methods: *reverse ray tracing* and *direct ray tracing* [11]. Reverse ray tracing is used to obtain the phase distribution to be applied in the array, whereas direct ray tracing is used to obtain the radiation pattern of the far field. As illustrated in Fig. 2(a), the rays at the lens output would not be parallel if the array is excited with a linear phase distribution and the resulting beam will be non-directive. Conversely, by exciting the array with the non-linear phase distribution derived from *reverse ray tracing*, the dome aperture exhibits parallel rays, as depicted in Fig. 2(b), indicating that a directive beam is realized. The amplitude distribution at the dome aperture is calculated by applying the principle of power conservation in ray tubes. As shown in Fig. 1, the k-ray tube is enclosed by the rays $\hat{\mathbf{s}}_{k-1}$ and $\hat{\mathbf{s}}_{k+1}$. The separation between the rays, or the width of the ray tube, is directly connected to the amplitude of the electric field at that location. Details on the calculation of this amplitude can be found in [19], [23]. Finally, the radiation pattern of the far field is computed making use of the Kirchhoff diffraction formula [19]. This formula assumes that the lens aperture is an array of radiating dipoles, where each point on the aperture contributes to the overall radiation.

Next, we investigate the integration of mutual coupling between array elements and interactions with dielectric materials into our 2-D ray-tracing model. This aims to more accurately simulate the behavior of PPAs when combined with domes. The resulting effects can significantly influence the performance of the array, particularly in terms of radiation patterns. Although the ray-tracing model discussed earlier effectively simulates an array of waveguides that resembles a continuous phase distribution [23], it encounters inconsistencies when the array comprises antenna elements such as patch antennas. In such scenarios, the array fails to mimic a continuous source, resulting in discrepancies between the ray-tracing model and full-wave simulations. To resolve this, we implement a radial configuration in the ray-tracing model, wherein rays are emitted radially from individual elements.

This modification represents the source as discrete elements instead of a continuum, thereby providing a more accurate system simulation. To account for mutual coupling, we will assign an amplitude to each ray according to its outgoing angle, which will be equivalent to the active element pattern of each array element when embedded in a dielectric material. For this study, we will use a patch antenna element from [27], where the profile is shown in Fig. 3(a). The patch is designed with two core substrates and a prepreg substrate. The two core substrates are made of Rogers 5880, with $\varepsilon_r = 2.2$ and $\tan\delta = 0.0009$, and their thicknesses are $h_1 = 1$ mm and $h_3 = 0.254$ mm, respectively. The prepreg substrate is Rogers 4450F, which has a $\varepsilon_r = 3.7$ and $\tan\delta = 0.004$, and its thickness is $h_2 = 0.1$ mm. The top and bottom views of the patch antenna are depicted in Fig. 3(b) and (c), respectively. The patch dimensions used are $w_{\text{patch}} = 4.52$ mm, $L_1 = 4.45$ mm, $L_2 = 6.9$ mm, and $L_3 = 2.4$ mm. Let us consider a simple array of five patch antennas separated $\lambda/2$, placed inside an infinite dielectric background of $\varepsilon_r = 3$ at a height of 0.1λ distance, as illustrated in Fig. 4(a). The active element patterns for this setup are shown in Fig. 4(b). To integrate the active element patterns obtained with a full-wave simulator into the ray-tracing model, we assign an amplitude to each ray that corresponds to the radiation pattern of the respective element. This method allows us to incorporate the effects of both mutual coupling and the nearby dielectric material.

III. Numerical Results

In this section, we validate our 2-D ray-tracing model by comparing the results with full-wave simulations performed using CST. The study is carried out on two different lens

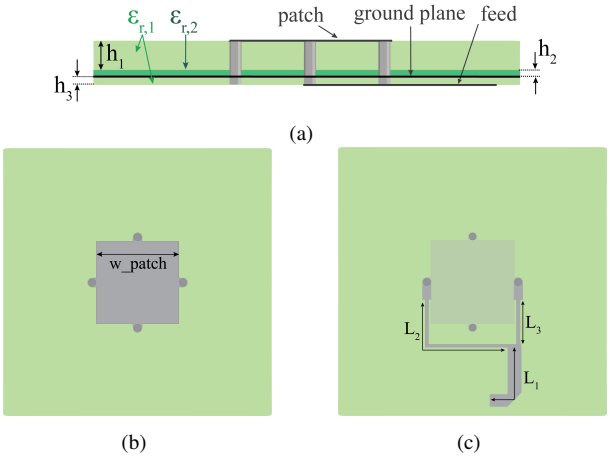

Fig. 3: (a) Profile, (b) top, and (c) bottom views of patch element.

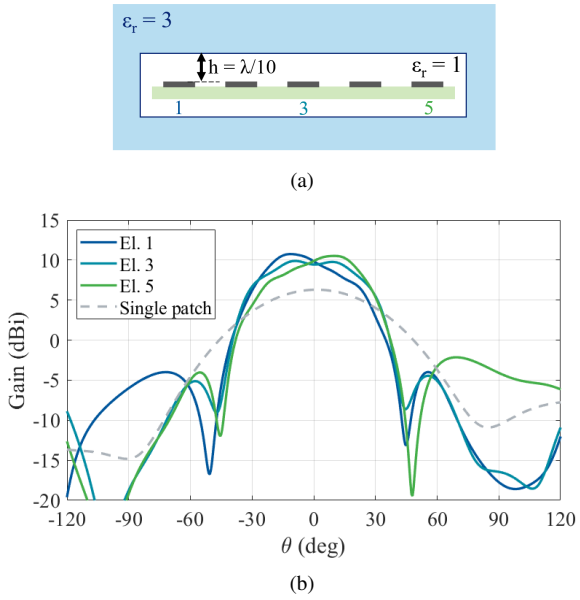

Fig. 4: (a) 5-element patch array within a dielectric background of $\varepsilon_r = 3$, and (b) active element patterns for elements 1, 3, and 5 compared with the radiation pattern of a single patch element.

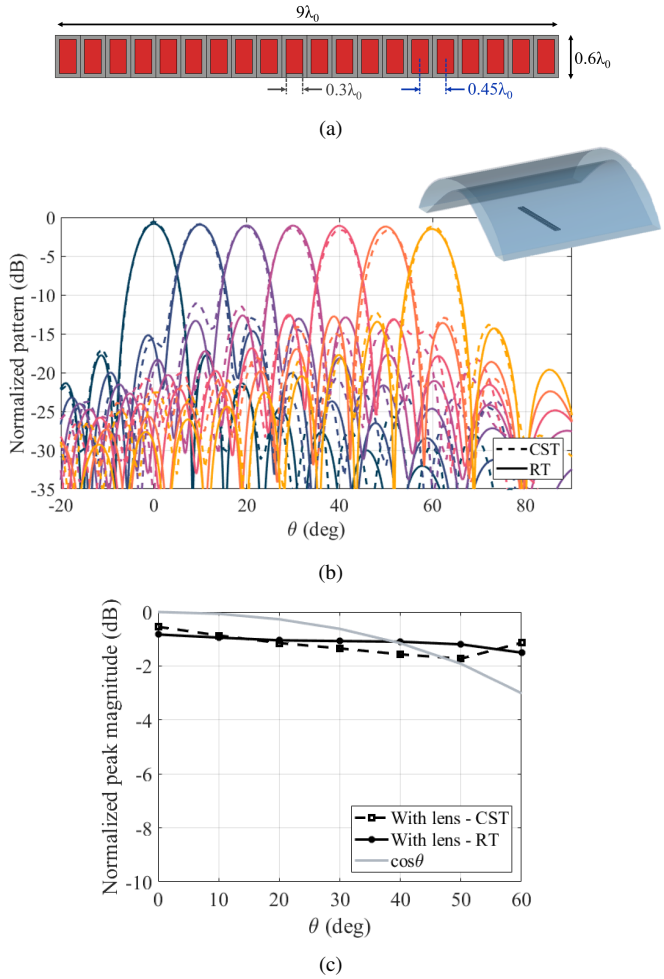

Fig. 5: (a) 20×1 waveguides array, (b) radiation patterns for the cylindrical lens on top of 20×1 array computed with 2-D ray tracing and CST, and (c) normalized peak magnitude.

geometries at 26 GHz: a cylindrical lens with a constant profile along the y-axis and a spherical lens rotationally symmetric with respect to the z-axis. For both cases, the lens profile is the same as shown in Fig. 1, and the parameters for S_1 and S_2 are those described in Section II. The dielectric constant of the lens is $\varepsilon_r = 2.5$, and matching layers are used to reduce reflection losses.

Initially, to validate the ray-tracing model, we analyze a scenario where the mutual coupling between the elements of the array is almost negligible; that is, a cylindrical lens covering a 20×1 waveguide array, as depicted in Fig. 5(a). The length of the lens in the y-axis is 250 mm. The phase distribution is obtained from the reverse ray tracing to achieve maximum directivity. The radiation patterns are shown in Fig. 5(b) for different angles from 0° to 60°. In this figure, we also compare the 2-D ray-tracing results with the full-wave CST simulations. The normalized peak magnitudes of the radiation patterns are shown in Fig. 5(c). The results in Figs. 5(b) and (c) are normalized to the broadside case without the lens. We can observe a good agreement between the data provided by our simplified 2-D ray-tracing model and CST, which clearly suggests that our 2-D ray-tracing tool effectively captures the radiation characteristics of the cylindrical lens, even for wide angles.

In a second example, we present the results for the spherical lens placed on top of the 20×6 waveguide array shown in Fig. 6(a). The radiation patterns are depicted in Fig. 6(b) where the ray-tracing and CST results are compared. The normalized peak magnitudes are presented in Fig. 6(c), with the results normalized to the broadside case with the lens. The ray-tracing results show again very good agreement with full-wave simulations, especially considering that we are comparing a 2-D model to simulate an inherently 3-D structure. Despite the increased complexity of the spherical lens, the 2-D ray-tracing tool effectively captures far-field behavior across the entire

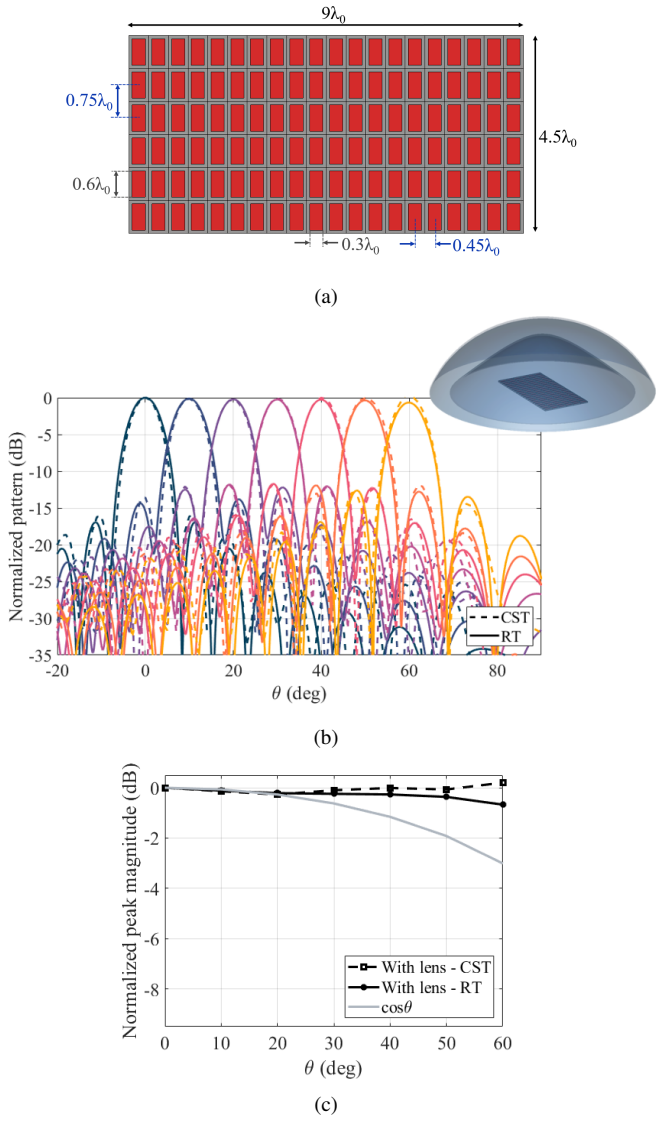

Fig. 6: (a) 20×6 waveguides array, (b) radiation patterns for the spherical lens on top of 20×6 array computed with 2-D ray tracing and CST, and (c) normalized peak magnitude.

scanning range. The simulation time required to compute the radiation pattern for one angle in ray tracing is about 240 times faster than that computed in CST for the cylindrical lens and 400 times faster for the spherical lens. This demonstrates that the 2-D model is not only computationally efficient, but also a reliable first step in the design process of 3-D dielectric dome antennas.

In the final analysis, we examine a scenario in which the impact of mutual coupling among the array elements becomes significant. Figure 7(b) and (c) present radiation patterns at two observation angles, 0° and 20°, for a 5-element patch array covered by a hemispherical radome with $\varepsilon_r = 3$ and a radius of $4.5\lambda_0$ at 25 GHz, as depicted in Fig. 7(a). The array is excited with a linear phase distribution in ray-tracing and CST. The radome is placed at $0.1\lambda_0$, increasing the influence of mutual coupling and dielectric effects. The antenna was

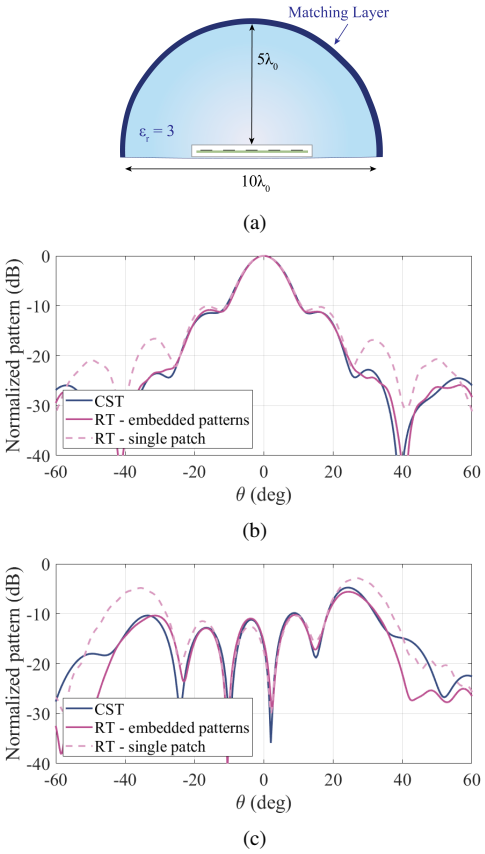

Fig. 7: (a) Dielectric hemispherical lens and radiation patterns at (b) 0° and (c) 20° for a 5-element patch array with a hemispherical radome of $\varepsilon_r = 3$ and a radius of 4.5λ. The patterns compare the results from CST, the 2-D ray-tracing model with embedded patterns, and the 2-D ray-tracing model using single-patch patterns.

simulated with the ray-tracing tool using two configurations: The first incorporates the embedded active element patterns from Fig. 4(b), while the second uses the single-patch element pattern in vacuum. These two cases are compared with full-wave CST simulations to validate the accuracy of the ray-tracing model. The comparison reveals that integrating embedded patterns into the ray-tracing model yields an improved correlation with CST results, especially at angles farther from the main beam. This highlights the significance of accounting for mutual coupling and dielectric effects and demonstrates the feasibility of incorporating these elements into a simplified ray-tracing model.

IV. Conclusion

In this work, we have demonstrated that a 2-D ray-tracing model can accurately predict the radiation characteristics of 3-D dome arrays, also when accounting for mutual coupling effects. The numerical results obtained from the ray-tracing simulations show a great agreement with full-wave CST simulations, even for complex geometries. The proposed model offers a significant reduction in computational time, making it a suitable first step in the design of practical 3-D antenna systems.

ACKNOWLEDGMENT

The contribution of M. Pubill-Font and C. Ding has been funded by Australian Research Council (ARC) DECRA under grant DE200101347. The work of F. Mesa has been partially supported by the grant PID2020-116739GB-I00 funded by MCIN/AEI/10.13039/501100011033. The work of A. Algaba-Brazález is supported by the Grant RYC2022-037385-I funded by MICIU/AEI /10.13039/501100011033 and by European Union NextGenerationEU/PRTR. The contribution of O. Quevedo-Teruel has been funded by the strategic innovation program Smarter Electronics System –a joint venture of Vinnova, Formas and the Swedish Energy Agency, under project 2023-00648.

REFERENCES

[1] M. Giordani, M. Polese, M. Mezzavilla, S. Rangan, and M. Zorzi, "Toward 6G networks: Use cases and technologies," *IEEE Commun. Mag.*, vol. 58, no. 3, pp. 55–61, 2020.

[2] W. Hong *et al.*, "The role of millimeter-wave technologies in 5G/6G wireless communications," *IEEE J. Microw.*, vol. 1, no. 1, pp. 101–122, 2021.

[3] Y. J. Guo and R. W. Ziolkowski, *Advanced antenna array engineering for 6G and beyond wireless communications*. John Wiley & Sons, 2021.

[4] T. Chaloun *et al.*, "Electronically steerable antennas for future heterogeneous communication networks: review and perspectives," *IEEE J. Microw.*, vol. 2, no. 4, pp. 545–581, 2022.

[5] O. Zetterstrom, J. Rico-Fernández, J. L. Gómez-Tornero, and A. Algaba-Brazález, "Industrial evolution of lens antennas towards 6G radio access applications," *IEEE Antennas Wireless Propag. Lett.*, pp. 1–5, 2024.

[6] Y. J. Guo, M. Ansari, R. W. Ziolkowski, and N. J. Fonseca, "Quasi-optical multi-beam antenna technologies for B5G and 6G mmWave and THz networks: A review," *IEEE Open J. Antennas Propag.*, vol. 2, pp. 807–830, 2021.

[7] O. Quevedo-Teruel, M. Ebrahimpouri, and F. Ghasemifard, "Lens antennas for 5G communications systems," *IEEE Comm. Mag.*, vol. 56, no. 7, pp. 36–41, Jul. 2018.

[8] M. Li, S.-L. Chen, Y. Liu, and Y. J. Guo, "Wide-angle beam scanning phased array antennas: A review," *IEEE Open J. Antennas Propag.*, 2023.

[9] S. Wang and G. M. Rebeiz, "Dual-band 28-and 39-GHz phased arrays for multistandard 5G applications," *IEEE Trans. Microw. Theory Techn.*, vol. 71, no. 1, pp. 339–349, 2022.

[10] A. Algaba-Brazález, P. Castillo-Tapia, M. C. Viganó, and O. Quevedo-Teruel, "Lenses combined with array antennas for the next generation of terrestrial and satellite communication systems," *IEEE Commun. Mag.*, vol. 62, no. 9, pp. 176–182, 2024.

[11] E. Gandini *et al.*, "A dielectric dome antenna with reduced profile and wide scanning capability," *IEEE Trans. Antennas Propag.*, vol. 69, no. 2, pp. 747–759, 2020.

[12] Y. Wan *et al.*, "Phased array antenna with top-truncated dome lens for wide-angle scanning," *IEEE Trans. Antennas Propag.*, vol. 72, no. 6, pp. 5066–5077, 2024.

[13] H. Zhang, S. Bosma, A. Neto, and N. Llombart, "A dual-polarized 27 dBi scanning lens phased array antenna for 5G point-to-point communications," *IEEE Trans. Antennas Propag.*, vol. 69, no. 9, pp. 5640–5652, 2021.

[14] H. Wang *et al.*, "6G energy-efficient systems based on arrays combined with dielectric lenses," *Elect. Lett.*, vol. 59, no. 17, p. e12932, 2023.

[15] G. A. Deschamps, "Ray techniques in electromagnetics." *Proceedings of the IEEE*, vol. 60, pp. 1022–1035, 1972.

[16] R. Brem and T. F. Eibert, "Multi-radiation center transmitter models for ray tracing," *IEEE Trans. Antennas Propag.*, vol. 60, pp. 3382–3388, 2012.

[17] M. M. Taygur, I. O. Sukharevsky, and T. F. Eibert, "A bidirectional ray-tracing method for antenna coupling evaluation based on the reciprocity theorem," *IEEE Trans. Antennas Propag.*, vol. 66, pp. 6654–6664, 12 2018.

[18] R. Brem and T. F. Eibert, "A shooting and bouncing ray (SBR) modeling framework involving dielectrics and perfect conductors," *IEEE Trans. Antennas Propag.*, vol. 63, pp. 3599–3609, 8 2015.

[19] Q. Liao *et al.*, "Ray-tracing model for generalized geodesic multiple beam lens antennas," *IEEE Trans. Antennas Propag.*, vol. 71, no. 3, pp. 2640–2651, 2023.

[20] F. Mesa, M. Chen, P. Castillo-Tapia, and O. Quevedo-Teruel, "Physical optics applied to parallel-plate lens antennas," *IEEE Open J. Antennas Propag.*, vol. 5, no. 4, pp. 833–844, 2024.

[21] I. Gashi, A. Paraskevopoulos, S. Maci, and M. Albani, "GO analysis of GRIN lens antennas by combining in a single ODE, field and wavefront-curvature transport to the ray-tracing," *IEEE Trans. Antennas Propag.*, pp. 1–1, 2024.

[22] M. Chen, O. Habiboglu, F. Mesa, and O. Quevedo-Teruel, "Ray-tracing and physical-optics model for planar Mikaelian lens antennas," *IEEE Trans. Antennas Propag.*, vol. 72, no. 2, pp. 1735–1744, 2024.

[23] M. Pubill-Font, F. Mesa, A. Algaba-Brazález, S. Clendinning, M. Johansson, and O. Quevedo-Teruel, "2-D ray-tracing model for multilayer dielectric dome arrays with inner reflections," *IEEE Open J. Antennas Propag.*, vol. 5, no. 4, pp. 845–854, 2024.

[24] L. Giupponi *et al.*, "Sub-band full-duplex for 5G new radio: Challenges, solutions and performance," in *2023 57th Asilomar Conference on Signals, Systems, and Computers*, 2023, pp. 167–173.

[25] 3rd Generation Partnership Project (3GPP), "3GPP Technical Report TR 38.858 Study on evolution of NR duplex operation (Release 18," 2023, accessed on June, 2023. [Online]. Available: https://www.3gpp.org/technologies/rel-18-duplex-ran1

[26] M. Born and E. Wolf, *Principles of Optics: Electromagnetic Theory of Propagation, interference, and diffraction of light*, 6th ed. Pergamon Press., 1964.

[27] F. Zeng, C. Ding, and Y. J. Guo, "A reconfigurable millimeter-wave antenna array with wide-range continuous beamwidth control (wcbc) based on polarization-mixing," *IEEE Trans. Antennas Propag.*, vol. 72, no. 4, pp. 3092–3103, 2024.